INT. J. NUM. METH. HEAT FLUID FLOW, VOL. 5, 889–905 (1995)

NUMERICAL SIMULATIONS OF A THREE-DIMENSIONAL NOZZLE, FROM INVISCID TO TURBULENT FLOWS

S. AUBERT, L. HALLO, P. FERRAND AND M. BUFFAT

Ecole Centrale de Lyon/Université Claude Bernard—Lyon 1, Laboratoire de Méchanique des Fluides et d'Acoustique (LMFA), URA CNRS 263, Ecole Centrale de Lyon, 36, avenue Guy de Collongue, BP 163, 69131 ECULLY CEDEX, France

ABSTRACT

Two numerical methods, based on high order finite volume formulations and upwind schemes, are used to compute the two- and three-dimensional flow field in a transonic nozzle. The influence of numerical diffusivity, boundary treatment and mesh structure is explored for inviscid and turbulent configurations. First order computations provide significantly different inviscid results. However, high order methods lead to similar solutions. An explanation of the error generated through the shockwave is proposed in this case. The two-dimensional interaction of the shock with the thin turbulent boundary layer developing on the bump wall is also presented. Good agreement between both approaches is obtained considering the rapid thickening of the boundary layer due to the shock. Furthermore, the downstream velocity recovery is almost identical. Only slight discrepancies occur in the main flow, near the outer edge of the boundary layer. These seem to be related to the way the turbulence model deals with the free stream turbulence. Finally, preliminary three-dimensional unstructured turbulent results are presented and discussed.

KEY WORDS Finite volume Upwind scheme Transonic Inviscid Turbulent

INTRODUCTION

Two CFD programs based on high order finite volume formulations and flux vector splitting have been developed at the LMFA[1]. These were designed to treat transonic flows, described by the Navier–Stokes equations, in two or three dimensions. It was required that the methods could accurately resolve shocks, and their interactions with walls and boundary layers. The methods used are currently well known, but the present work offers coherent solutions in applied CFD, from spatial discretization, through flux vector splitting, to boundary condition treatments.

Our purpose is to compare both approaches, their accuracy and their flaws, through an inviscid and turbulent gas dynamic problem derived from the Adamson nozzle[2].

DESCRIPTION OF THE NUMERICAL METHODS

The first method is designed to compute three-dimensional unsteady flows in turbomachinary where interactions of waves and aeroelastic coupling between flow and blades occurs[1]. It is based on a MUSCL finite volume formulation[3] over moving structured meshes. It uses the Van Leer flux vector splitting technique, with the Mulder limiter which controls spatial accuracy in the vicinity of discontinuities[4]. It is hybridized according Mach Number with a classical centred scheme to circumvent its poor behaviour near no-slip walls[5]. The viscous terms are computed by a second order centred scheme, and turbulence effects are described by a basic algebraic eddy viscosity model[6]. Natural boundary conditions, including symmetry, slipping walls and non

0961–5539/95/100889–17$2.00

Received February 1994
Revised July 1994

reflective conditions, are implemented by mean of compatibility relations, using the interior time scheme[7]. The time discretization involves the explicit forward Euler formula. The whole scheme is built to ensure coherence in time with particular attention being paid to avoiding numerical phase differences for the transient solution. It is subsequently referenced as the *structured* or *Van Leer* approach.

The aim of the second method is to provide a means of predicting steady two and three-dimensional internal turbulent transonic flows involving chemical reactions[8]. To take into account complex geometries and to allow local grid refinement, unstructured finite element meshes are used. The finite volume integration cells are built around each node by means of the medians[9]. The approximate Riemann solver of Roe with the Van Albada limiter is employed. The diffusive and source terms are integrated using a Galerkin finite element formulation, with mass lumping approximation for time integration[10]. A classical high Reynolds number k-ε model[11] and wall laws are used to model turbulent flows[12]. A linearized implicit time scheme is employed to accelerate the convergence towards the steady-state solution[13,14]. This is based on a first order Taylor expansion in time of the conservation equations. Inviscid terms are computed along edges using the jacobian matrix expression of Steger and Warming, and the viscous effects are linearized according to a finite element approach[15,16]. Local time stepping is employed such that at each node the solution is allowed to advance in time at the maximum rate compatible with a fixed CFL number and the size of the surrounding cell[17]. The boundary conditions are implemented using explicit compatibility relations[18], and a weak formulation, where fluxes on all boundaries are prescribed. This approach is subsequently referenced as the *unstructured* or *Roe* method.

DESCRIPTION OF THE TEST CASE

Both methods are used to compute inviscid and turbulent compressible steady flow fields in a three-dimensional nozzle. Its shape is a modified derivation of that used by Adamson and Liou[2], and it is extensively described by Ott, Bölcs and Fransson[19]. The geometry consists of a flat channel with 10% thick sinusoidal bumps on upper and lower walls. Its width is constant, and equals half of the inlet height. The problem is bi-symmetric with respect to the axis of the nozzle. A perspective view, including the three-dimensional mesh, is given in *Figure 1*. Using non-dimensional lengths, the nozzle is 2.0 long, 0.8 high and 0.4 wide. The bump is centred around $X=0.5$ and its overall length is 4/3.

The non-dimensional inlet conditions are such that the total pressure equals 0.9341, the total temperature is 0.7710 and there are no transverse velocity components. The inviscid outlet static pressure equals 0.6520, and it is lowered to 0.6350 in turbulent computations to ensure the same shock position on the axis in both cases. The flow is transonic, with a shock in the nozzle. Its position is visible in *Figure 2*, where iso-Mach number lines are plotted. The Mach number varies from 0.6 to 1.4.

The reference conditions are such that the length is 0.1 m, the velocity is $358.58\ \mathrm{m\,s^{-1}}$, and the density equals $1.3926\ \mathrm{kg\,m^{-3}}$. The specific heat ratio is $\gamma=1.4$, and the perfect gas constant equals $r=287\ \mathrm{J\,kg^{-1}\,K^{-1}}$. The turbulent Reynolds number is 10^6.

A typical two-dimensional inviscid structured mesh with 82×26 nodes, is shown in *Figure 3*. The finite element mesh is obtained by dividing each quadrangle into two triangles in two dimensions, and each hexahedron into six tetrahedrons in three dimensions. The upper boundary is treated as a wall, with either slip or no-slip conditions. The lower boundary is always treated as an axis of symmetry. The mesh is adapted around the shock position, with a longitudinal ratio of 10 between the longest and the shortest cells. On the other hand, the transversal cell size is function of a geometric ratio, from 1.1 for inviscid computations to 1.3 for turbulent computations.

Profiles of representative variables are subsequently presented. In each figure, profiles along the axis of the nozzle are in the lower left corner, with the related rules; while profiles on the

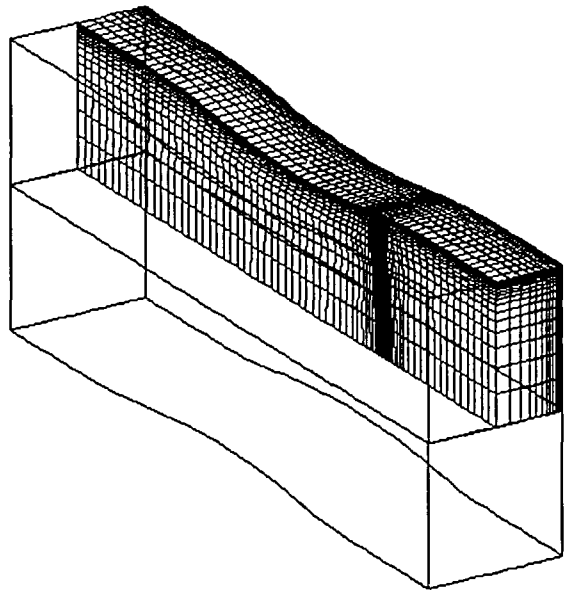

Figure 1 Nozzle shape, including the three-dimensional structured mesh

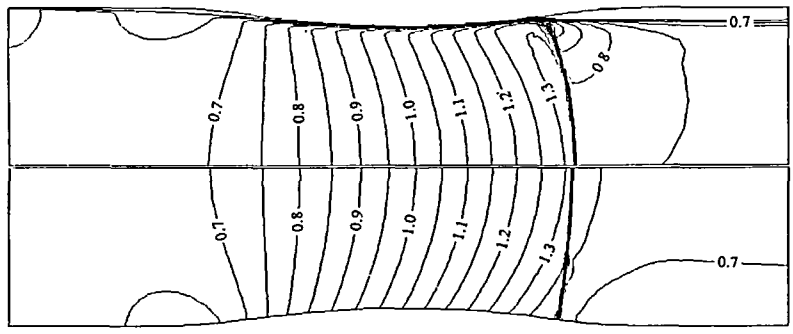

Figure 2 Iso-Mach number lines. Up: Roe Turbulent. Down: Roe Inviscid

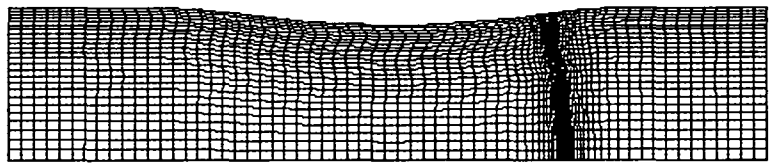

Figure 3 Structured half nozzle geometry

bumped wall are plotted in the upper corner, with the abscissa rule printed on the top of the figure and the ordinate rule printed on the right. The non-dimensional static pressure is displayed, while what is referenced as the total pressure is the difference between the local total pressure and the inlet total pressure, non-dimensionalized by the inlet total pressure.

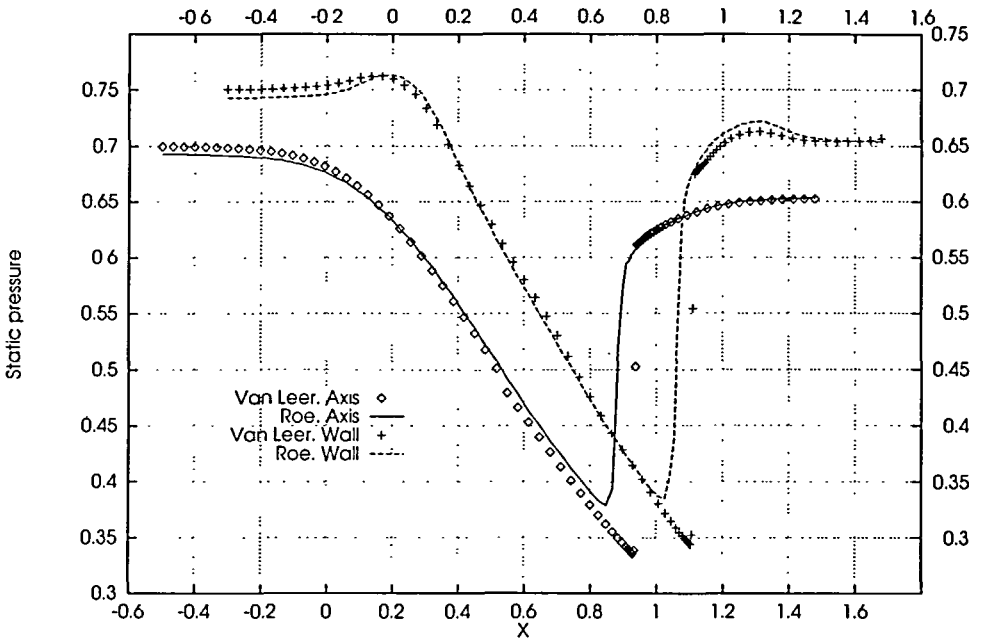

Figure 4 First order inviscid static pressure profiles

INVISCID COMPUTATIONS

As the lateral walls are flat, the inviscid flow is two-dimensional with no variations in the width direction. In this case, true two-dimensional unstructured computations were thus performed, while a three-dimensional mesh with only two layers of cells and symmetry conditions in the non-revealing direction, were used for structured simulations. The inlet flow field was assumed uniform.

First order inviscid computations

Previous comparisons of first order inviscid computations of shock tube flow problems revealed only slightly different results[1], but this is not a general conclusion. In this nozzle test case, the static pressure profiles obtained are quite different (*Figure 4*). The unstructured method computes a more diffuse shock, upstream of the position found by the structured approach. Inlet static pressures are lower, while outlet static pressures and inlet total pressures, which are imposed boundary conditions, are well preserved. Considering the total pressure profiles (*Figure 5*), the same behaviour is noticeable. Whereas total pressure should be constant for isentropic flows, i.e. upstream and downstream to the shock, errors of 2% or 3% are introduced by both methods, mainly near the curved wall. In the convergent part of the nozzle, the total pressure is overestimated, while it is underestimated in the divergent section. Since numerical losses cause a reduction in total pressure upstream of the shockwave, and the exit static pressure is unchanged, the shockwave position is shifted towards the inlet. As the error due to the unstructured approach is the biggest (higher than 4%), the computed shock is on the left of the one found by the structured method with an error of 2%. A puzzling result is noticeable on the total pressure profiles (*Figure 5*). Both methods exhibit an undershoot at the shock position, which is surprising for first order accurate schemes in space, presumed to produce monotone solutions. This behaviour exists along the shock, from the axis to the wall.

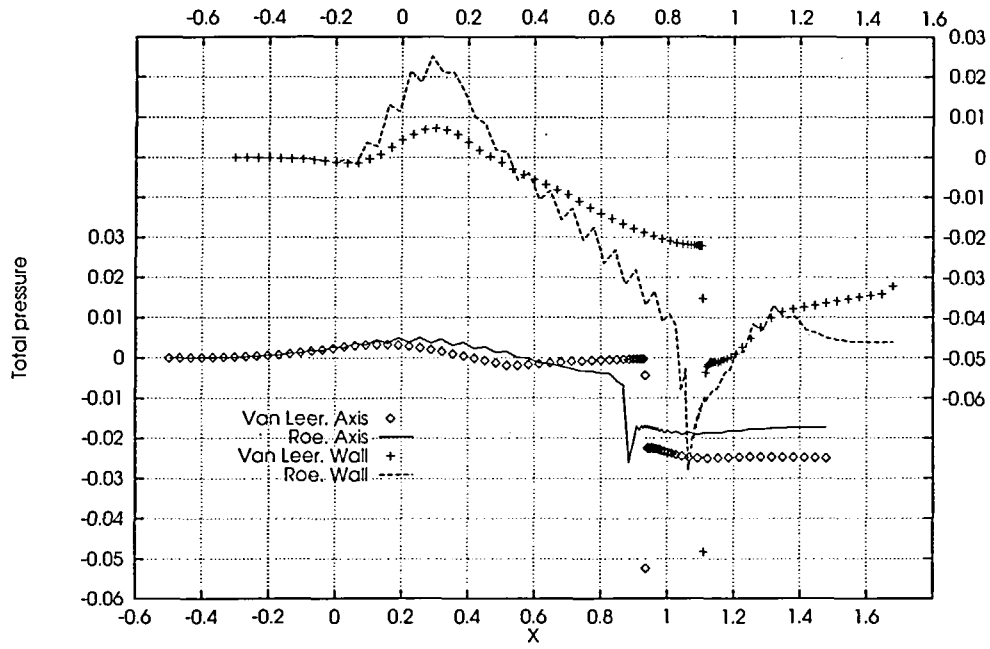

Figure 5 First order inviscid total pressure profiles

The flow fields computed with first order schemes exhibit the right behaviour, but the errors, mainly on total pressure levels, make them unreliable for quantitative comparisons, if not for qualitative ones. Furthermore, significant differences were noticed between the two approaches.

High order inviscid computations

The spatial accuracy in the following results has been increased to second order. The static pressure profiles are shown in *Figure 6*. In this case, the results are similar, with differences much smaller than those found in the first order computations (*Figure 4*). The profiles are nearly the same on the axis where the flow field is one-dimensional, and they are close to the one-dimensional analytical solution. However, there are greater differences on the wall, where the curvature of the upper boundary influences the pressure distribution. It seems the two methods do not handle curvature in the same way. The unstructured shock is again located upstream of the structured one, but by just one cell this time. Because of the size of the local adapted cells, this difference is negligible. Furthermore, it does not occur as a result of the different limiters: the expressions given by Mulder and by Van Albada are similar, and it was verified that the layout of first order nodes, and the intensity of the limiters are identical in the shock vicinity using those two expressions.

The Mach number varies from 0.66 to 1.3 then down to 0.71 on the axis, while it is up to 1.4 on the wall. This variation generates different jumps of total pressure across the shock, which are respectively of 2.5% and of 3.5% (*Figure 7*). In this case, the total pressure is well conserved in isentropic regions, with only slight differences between the two approaches. The outlet total pressure levels predicted by each method are equal. It will be noticed that there are still over- and undershoots in the shock vicinity.

These results establish that the approaches compute similar two-dimensional inviscid solutions as long as high order spatial schemes are used. Subsequent calculations presented in the paper are based on high order schemes. However, the error generated by such schemes within shockwaves is borne in mind.

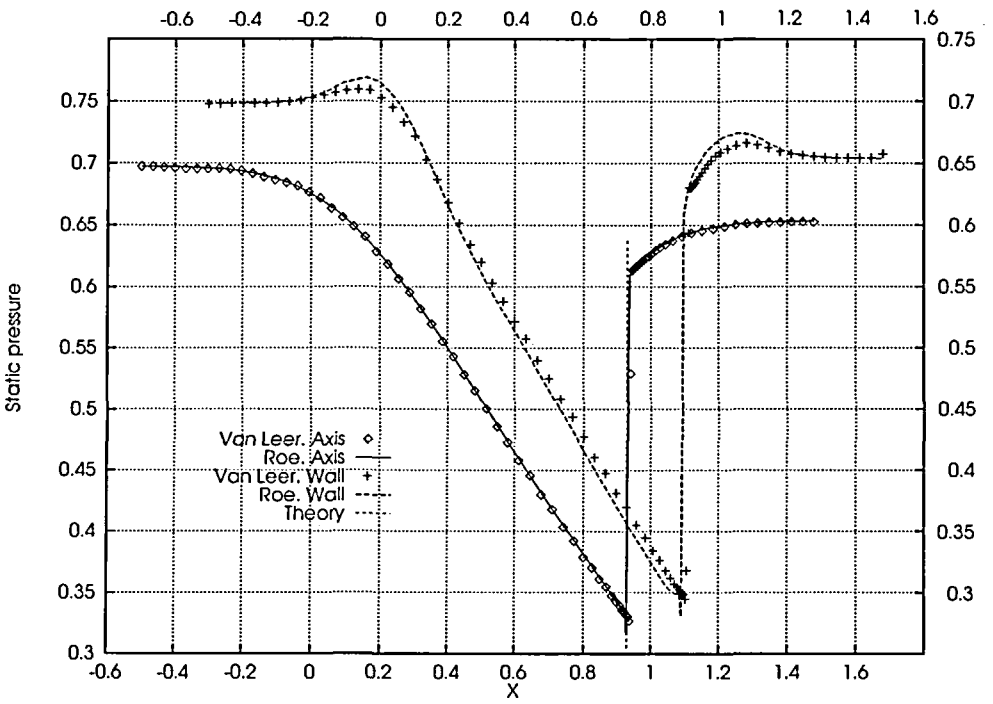

Figure 6 Second order inviscid static pressure profiles

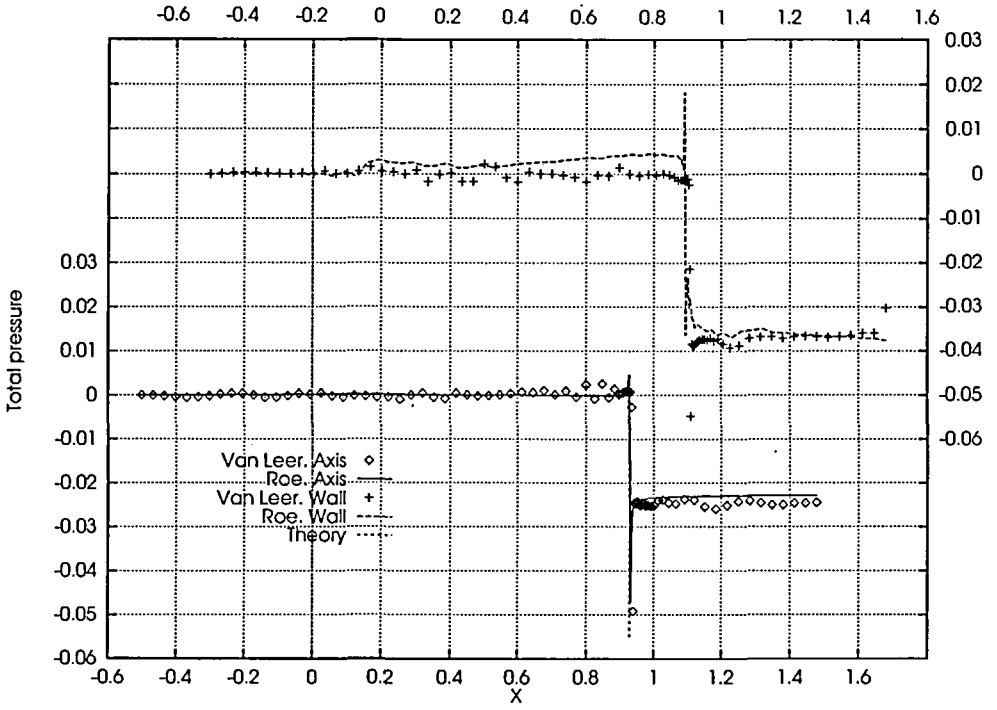

Figure 7 Second order inviscid total pressure profiles

ERROR ON THE SLIP CONDITION

Significant errors in shock position and total pressure profiles near the upper boundary were noticed for first order unstructured results (*Figures 4* and *5*). Two arguments could explain this. On the one hand, it is well known that for first order schemes, the Roe flux splitting computes more diffuse shocks than the Van Leer one, while it predicts sharper contact discontinuities[20]. On the other hand, the slip condition, and then the symmetry condition, implemented as a weak condition in the unstructured method lead to a non zero velocity normal to the walls. The dot product of the velocity and the unitary normal to the wall non-dimensionalized by the modulus of the velocity, is plotted in *Figure 8*, for first and second order accurate schemes in space. It shows that some fluid exits the computational domain in the convergent part of the nozzle. The noticeable oscillations seem to be related to those found on the total pressure profiles (*Figure 5*). These errors contribute undoubtedly to the variations of the total pressure, increasing the numerical losses, and then shifting the shock position. It was verified that the slip condition implemented in the structured approach does not produce such an error.

It will be noticed that the second order scheme is more accurate than the first order one. Indeed, the greater the number of nodes in the flux evaluation, the better the slip condition is enforced. However, there is still some fluid crossing the convergent wall. This problem could explain the overestimation of the upstream total pressure noticeable on the unstructured wall profile (*Figure 7*). Furthermore, the slip condition is not verified across the shock. This could be due to the weak approach used.

ERROR GENERATION THROUGH THE SHOCK

The results presented exhibit overshoots and undershoots across the shock, for structured and unstructured computations. This seems to be related to the generation of local errors when the Mach number varies from supersonic to subsonic. In this region, the upwinding changes and

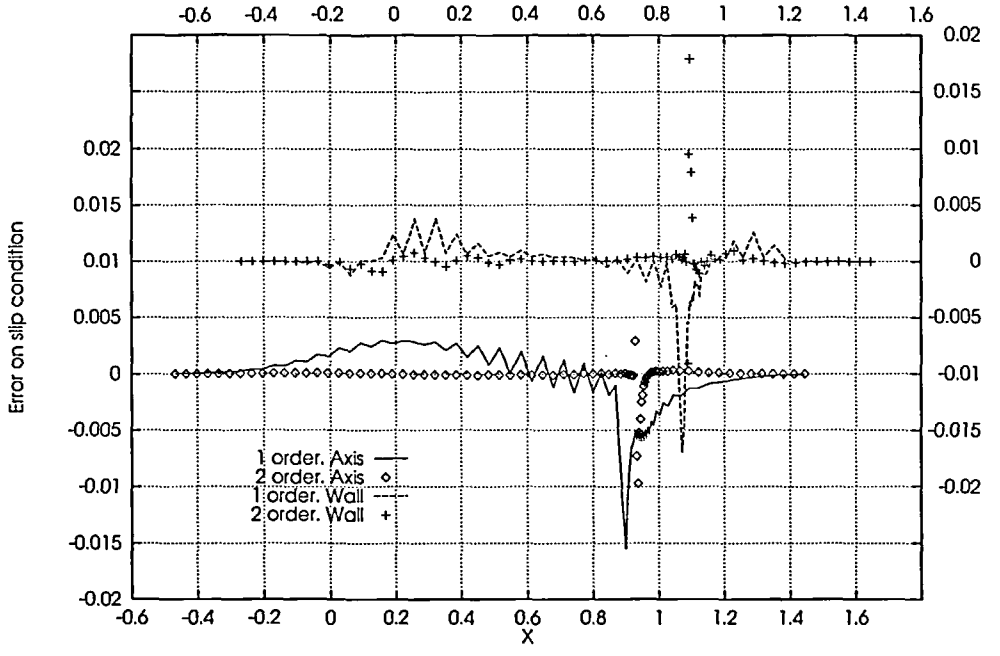

Figure 8 Error on unstructured slip condition

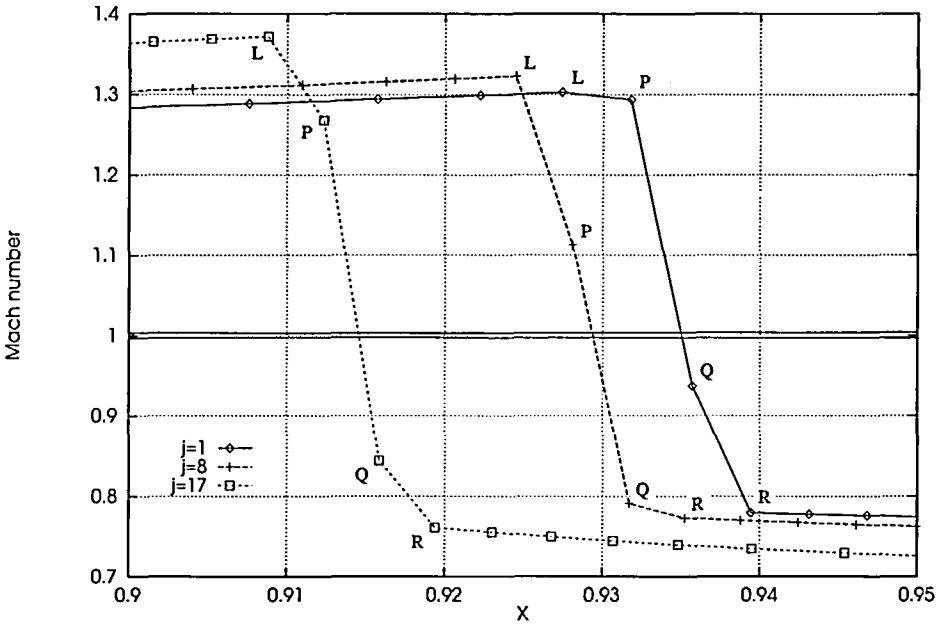

Figure 9 Structured Mach number profiles in the shock vicinity

the link between the zones is flawed. On the one hand, when the Mach number is higher than one, there is no upstream travelling information, and all the information is carried downstream. On the other hand, in the subsonic region, there are upstream and downstream travelling waves. Therefore because of the upwinding, there is one cell's interface between the zones, where supersonic downstream and subsonic upstream information are mixed in a non-physical way. As the inviscid steady state implies the conservation of flux through the cells interfaces, the finite volume formulations based on this property modify the flow field at the centre of the cells to enforce this conservation, even if non-physical nodal solutions are computed. In this way, over- or undershoots can locally arise.

To justify this, we subsequently demonstrate that it is not possible to conserve in the same time, the flux at the cells interfaces and at the nodes. We consider three mesh lines extracted at various height of the geometry, referenced as $j=1$, $j=8$ and $j=17$, for first order structured computations. Mach number profiles, around the shock position, are plotted on *Figure 9*, and the difference between the local total temperature and the inlet total temperature, non-dimensionalized by the inlet total temperature, is shown on *Figure 10*. This variable should be equal to zero for steady adiabatic flows. The following discussion is based on the argument of Van Leer dealing with how his flux splitting technique handles steady discontinuities[21]. The same notations are used. The supersonic pre-shock state is denoted L, the subsonic post-shock state R, and the interior states P and Q, such that zone P is supersonic and zone Q is subsonic. Considering *Figure 10*, we notice that errors occur only for nodes P and Q. Furthermore, the nearer to the sonic line these nodes are, the bigger the error. Variations upstream of L and downstream of R are due to the first order accuracy, and are not relevant to the above argument. Split fluxes in the flow direction, F^+ and F^-, are printed in *Table 1*, with $F_l^+ + F_r^-$, the built flux at each cells interface. For supersonic nodes, F^+ equals the full flux F and F^- is zero.

Let $\bar{F}$ be the flux imposed by the boundary conditions. L and R states are supposed known without errors, such that:

$$F(q_L) = F(q_R) = \bar{F} \tag{1}$$

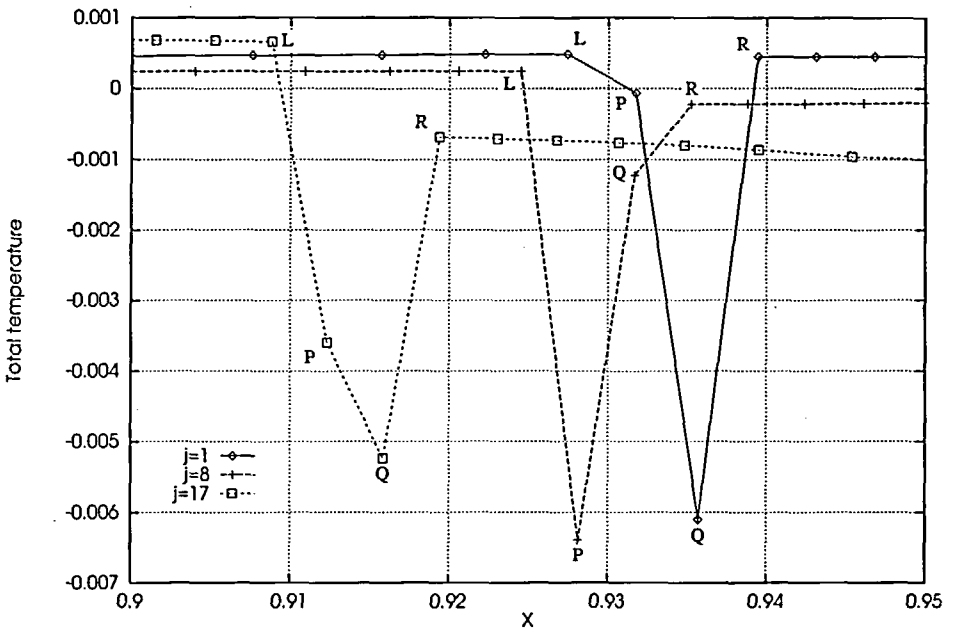

Figure 10 Structured total temperature profiles in the shock vicinity

Table 1 Split fluxes at nodes and at cells interfaces

Node	F^+	F^-	$F_l^+ + F_r^-$
L ($M>1$)	$F(q_L)$	0	$F(q_L)$
P ($M>1$)	$F(q_P)$	0	$F(q_P)+F^-(q_Q)$
Q ($M<1$)	$F^+(q_Q)$	$F^-(q_Q)$	$F^+(q_Q)+F^-(q_R)$
R ($M<1$)	$F^+(q_R)$	$F^-(q_R)$	

This hypothesis is valid if the differences of total temperature between points L and R are negligible (*Figure 10*).

At the interface PQ, we have:

$$F(q_P)+F^-(q_Q)=\bar{F} \tag{2}$$

On the other hand for the first order scheme:

$$F(q_R)=F^+(q_R)+F^-(q_R)=\bar{F} \tag{3}$$

so, the flux conservation at the interface QR:

$$F^+(q_Q)+F^-(q_R)=\bar{F} \tag{4}$$

is equivalent to:

$$F^+(q_Q)=F^+(q_R) \tag{5}$$

For a one-dimensional flow, (5) reduces from 3 to 2 independent scalar equations, the Van Leer split energy flux being a function of the split mass and momentum fluxes. So we end up with 5 equations, (2) and (5), for 6 unknowns, q_P and q_Q, with one parameter being the sub-grid shock position between P and Q. For multi-dimensional flows, the geometry of the nozzle, and the inlet and outlet boundary conditions, determine the shock position. So the momentum equations in the transverse directions replace the previous parameter. In three-dimensions, we end up with 10 equations for 10 unknowns.

If state P is such that the flux is conserved, $F(q_P)=\bar{F}$, then according to equation (2), $F^-(q_Q)=0$, which implies that $M(q_Q)>1$, whereas zone Q is supposed to be subsonic. Therefore, the flux could not be conserved for node P, and then for node Q. This shows that it is not possible to conserve the numerical flux at the same time at the cells interfaces and at the nodes, through a shock.

This argument is developed with the Van Leer flux vector splitting, but its conclusion is nevertheless more general, and it is valid for each method building independent left and right states for a cell interface, according to the Mach number at the cell centre. There will always be an error when the shock is crossed. The Roe splitting used in the unstructured approach shows the same behaviour.

It will be noticed that it was not possible to obtain convergence of the structured computation if the outlet static pressure was fixed. Non reflective outlet conditions had to be used[22]. This is related to the longitudinal oscillation of the shock between two cells, because of this error introduced by the flux splitting scheme across the shock. Transversal instabilities exist when the sub-grid shock position changes in the height of the nozzle. Waves are generated by this oscillation, and a coupling with the outlet appears, preventing convergence. Even in this case, small errors are visible on the total pressure levels (*Figure 7*). This drawback does not appear in the first order computation because of the significiant numerical viscosity which damps the oscillations. The implicit scheme in time used in unstructured computation has the same 'beneficial' influence, taking advantage of larger time steps.

TWO-DIMENSIONAL TURBULENT COMPUTATIONS

The next step involves the simulation of the transonic turbulent flow field in the previous two-dimensional geometry. The viscous boundary layer on the no-slip bump wall is now taken into account. Uniform inlet static pressure is imposed. The velocity is also assumed uniform throughout the height, except on the wall where it is zero. The total pressure profile is no longer uniform in order to include the inlet boundary layer. The total temperature is unchanged, but the outlet static pressure is decreased by 3% to counterbalance extra viscous losses and to ensure the same shock position on the axis (*Figure 2*).

Comparing iso-Mach number lines for inviscid and turbulent computations (*Figure 2*), we notice on the one hand that the core flow up to the half height is unchanged. On the other hand, differences are confined to near the wall, and mainly after the shock/boundary layer interaction which produces a low speed region downstream. Because the Mach number in the turbulent case is lower than 1.35, the pressure gradient induced by the shock contributes only to thicken the boundary layer, and no recirculation zone is generated. The total pressure levels exhibit the same behaviour (*Figure 11*). Along the axis the inviscid and turbulent results are similar, implying that viscous effects are negligible in this region. Losses in the boundary layer, however are around 40%, and its thickening downstream of the shock is evident. As the Mach number in the inviscid case increases from the axis to the wall due to curvature, the shock strength, and hence the pressure jump, also increases. The Mach number in the turbulent case increases up to the half height, and then decreases because of viscous effects. The total pressure jump shows the same trend. This explains why in the turbulent case losses are lower near the boundary layer.

The structured simulation is performed using a mixed scheme which hybridizes according

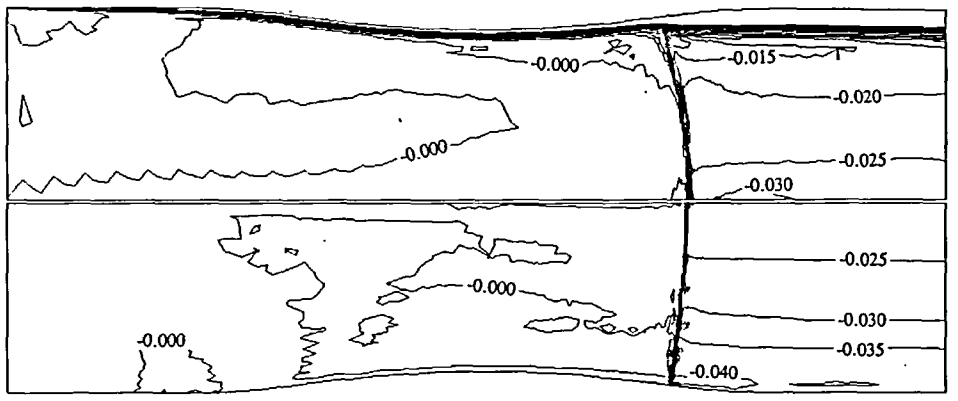

Figure 11 Iso-total pressure lines. Up: Roe Turbulent. Down: Roe Inviscid

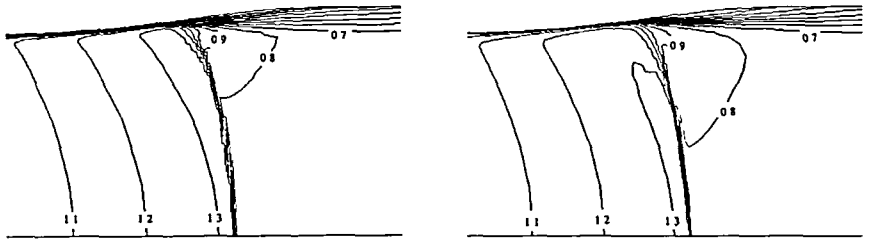

Figure 12 Turbulent iso-Mach number lines. Left: Van Leer. Right: Roe

Mach number the Van Leer flux vector splitting technique and a classical centred scheme[5]. For Mach numbers higher than 0.6, the Van Leer scheme is used alone, whereas at Mach zero, only the centred scheme is effective, with a smooth transition from $M=0.6$ to $M=0.0$. The explicit artificial dissipation required at low Mach numbers is set to one twentieth of its maximum value. The non-slip condition is imposed at the wall. For the unstructured computation, the inlet k and ε levels are supposed constant, and are evaluated from a free stream turbulence level of 4%. A small wall distance of 8.10^{-5} has been chosen for the upper wall, to ensure a good description of the turbulent boundary layer by the wall laws.

The aim is to compare the two methods when turbulent effects are included, knowing that the flow fields achieved by high order inviscid computations were very similar.

Mach number levels are plotted in *Figure 12*. Slight differences are visible on iso-lines 1.1 and 1.2 which are more rounded near the wall for unstructured results, and the very low speed region downstream of the shock is shorter in the structured calculations. The main discrepancies however are in the shock vicinity. From three quarters of the height to the edge of the boundary layer, the iso-line 1.3 is substantially different. In this region, the unstructured Mach number is lower, so the shock is weaker, and the downstream velocity higher. The iso-line 0.8 being shifted to the right is then coherent. The total pressure levels are in agreement with these results (*Figure 13*). Whereas the levels are close near the axis, the jump across the shock in the boundary layer vicinity is lower in the unstructured simulation, characterizing a weaker shock. It thus appears that the k-ε model is more diffusive near the outer edge of the boundary layer. This can be explained by the imposed free stream turbulence that is required at inlet. Indeed, the algebraic model used in the structured computation is effective only inside the boundary layer, whereas the k-ε model acts everywhere that gradients are significant, particularly in the vicinity of the.

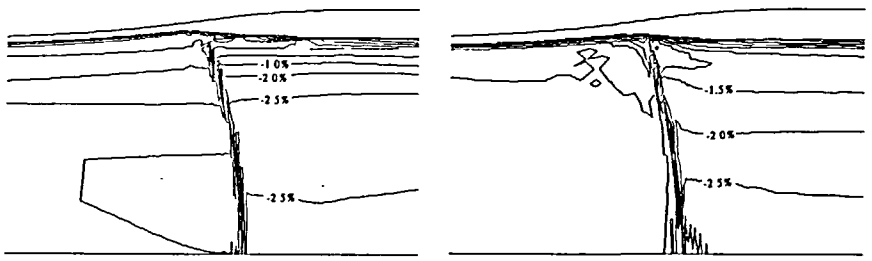

Figure 13 Turbulent iso-total pressure lines. Left: Van Leer. Right: Roe

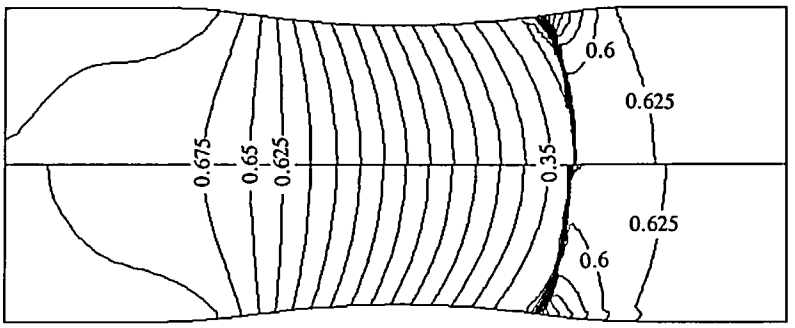

Figure 14 Turbulent iso-static pressure lines. Up: Van Leer. Down: Roe

boundary layer. The lower the free stream turbulence level is, the lower the dissipation should be. This assumption has not been checked yet, but some verifications are in progress.

Considering the iso-static pressure lines (*Figure 14*), we see very good agreement between the approaches, mainly from the inlet to the shock, where the turbulence influence is small and the flow nearly inviscid. The only significant differences are in the vicinity of the shock/boundary layer interaction due to the shock strength variations previously described. The static pressure profiles along the bump exhibit the same behaviour (*Figures 15* and *16*). It will be noticed that the unstructured shock is shifted to the left, which is consistent with a lower Mach number, and that the post-shock pressure rise is slower, consistent with a longer low velocity region after the shock.

Velocity profiles at the throat are given in *Figure 17*, $Y=0.355$ being the half throat height. For the unstructured calculations, wall laws are used to compute a friction velocity, $V_w \simeq 0.5$ at $Y_w=0.355$, which is half of the free stream velocity, $V \simeq 1.0$ at $Y=0.0$. This may explain the differences between the results for $Y \in [0.35; 0.355]$. Otherwise, there is a very good agreement in this location, where the flow is nearly inviscid with a very thin boundary layer. The same data near the outlet are plotted in *Figure 18*. At this location, the velocity profile for $Y \in [0.35; 0.39]$ is distorted, due to the shock/boundary layer interaction which induces a velocity defect. The methods predict nearly the same velocity distribution. In the structured calculations, the velocity recovers just a bit faster, which is consistent with a shorter low velocity region after the shock.

According to these results, we can state that both approaches are able to compute the interaction of the shock with the thin boundary layer developing on the bump. The calculated flow fields are fairly similar, and consistent from a physical point of view. The slight discrepancies noticed should be related to the models of turbulence used, which unfortunately strongly affect the numerical simulation. It appears that the free stream turbulence level modifies the near boundary

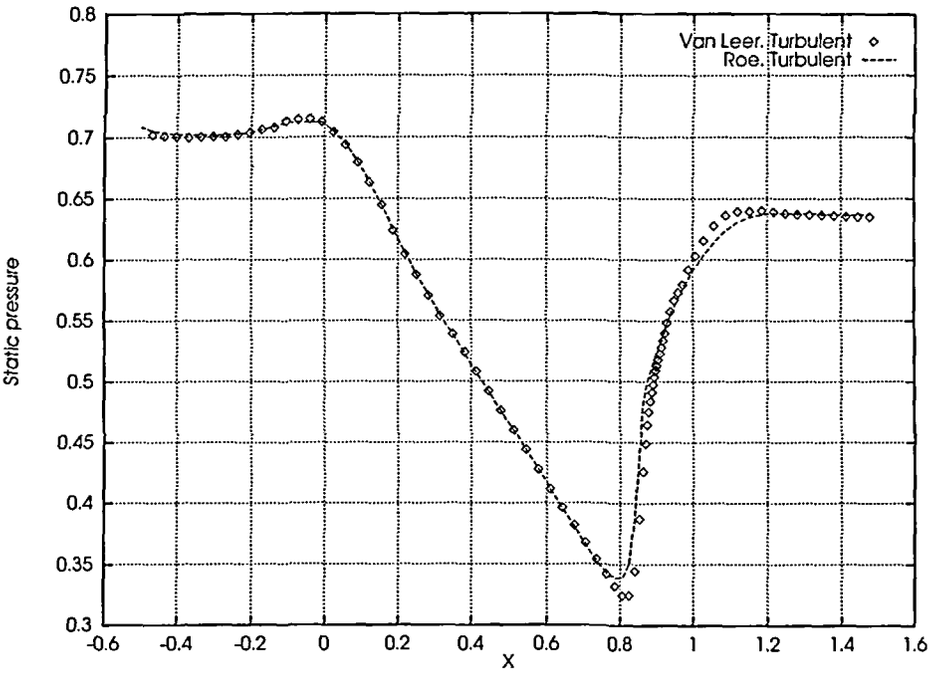

Figure 15 Turbulent static pressure profiles along the bump

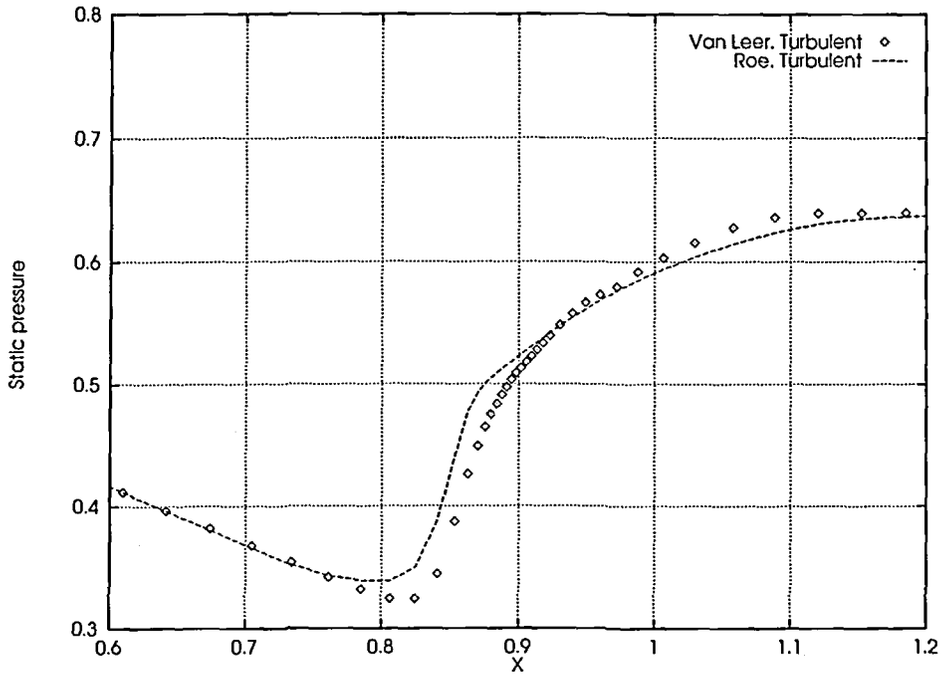

Figure 16 Turbulent static pressure profiles along the bump (detail)

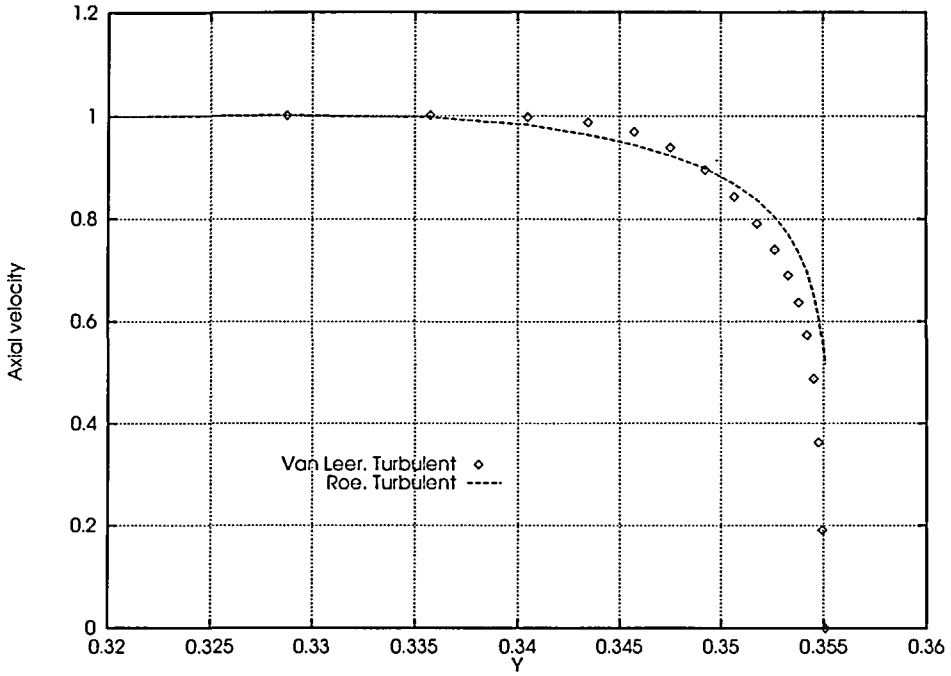

Figure 17 Turbulent velocity profiles at the throat

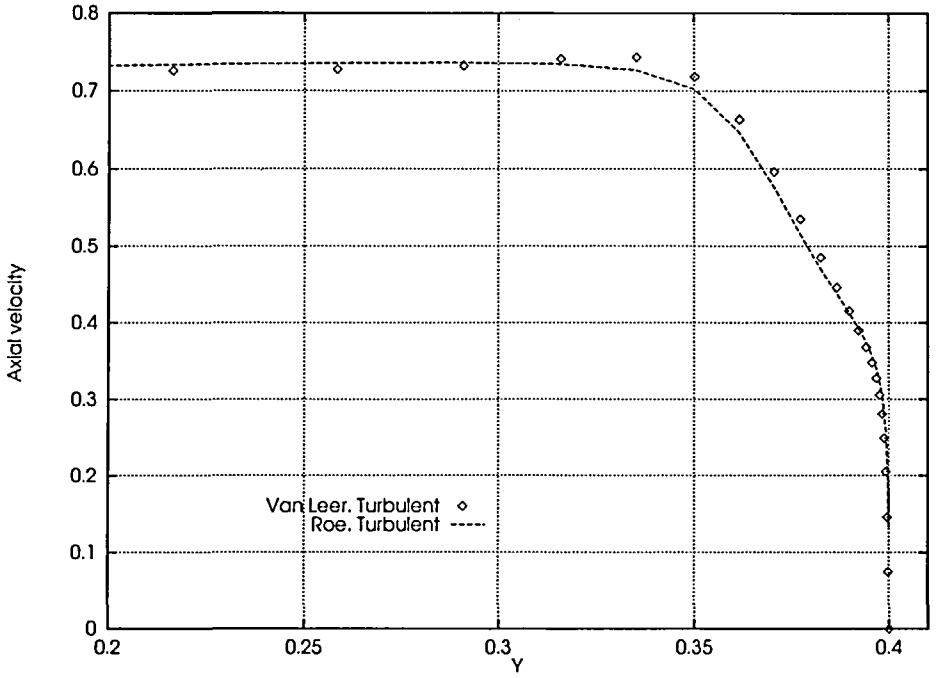

Figure 18 Turbulent velocity profiles at the outlet

layer region when the k-ε model is used. On the other hand, the algebraic model appears to produce a higher level of eddy viscosity, which damps more quickly the influence of the shock/boundary layer interaction.

THREE-DIMENSIONAL TURBULENT COMPUTATIONS

Last step involves the simulation of the transonic turbulent flow field developing in the three-dimensional geometry (*Figure 1*). No-slip boundary are imposed on the bump and on the lateral flat wall, and slip conditions are imposed on the two planes of symmetry. The inlet and outlet boundary conditions are unchanged compared to those of the two-dimensional turbulent computations, except the inlet velocity profile, which now takes into account a very thick boundary layer on the lateral flat wall. Its initial thickness equals 0.1.

Only unstructured results are available until now, and are presented here as preliminary ones. These are compared with the previous two-dimensional turbulent unstructured solution. The iso-static pressure lines in the vertical plane of symmetry are presented in *Figure 19*. They are similar to those shown in *Figure 14*, which indicates that the flow is quasi-bidimensional in the vicinity of this section. This is not surprising because the thick boundary layer does not reach the core of the nozzle even though it becomes larger in the interaction zone with the shock. On the other hand, in the corner of the two solid walls, there is a strong interaction between the shock and the boundary layers, which induces the formation of a three-dimensional vortex with a large spreading of the initial inviscid shock. This is shown in *Figure 20*, which presents the iso-static pressure values on the boundaries of the computation domain. Further comparisons are, however, necessary to validate those complex three-dimensional structures and this preliminary solution.

CONCLUSION

Two numerical methods based on high order finite volume formulations and upwind schemes were used to compute the two- and three-dimensional steady flow field in a transonic nozzle. Previous comparisons on shock tube problems had produced similar results for the two schemes. Our present purpose was to extend this work to the calculation of a more complex situation.

Inviscid computations were carried out with first order accurate schemes in space. They provided significantly different results. The chosen flux splitting, and the slip condition treatment, may explain this behaviour. Furthermore, we have attempted to understand the mechanism generating numerical errors within a shock wave.

On the other hand, the two approaches produced very similar results when higher order schemes

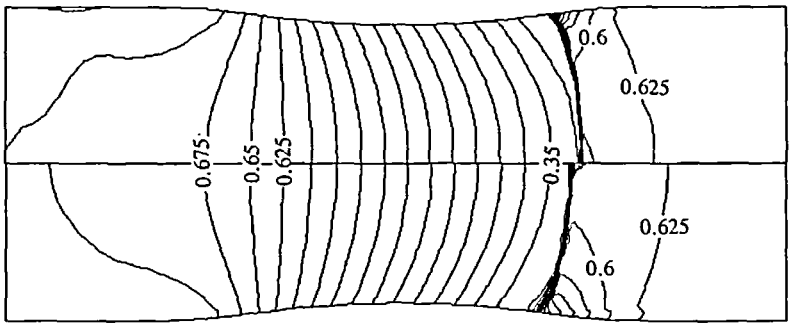

Figure 19 Turbulent iso-static pressure lines. Up: Roe 3D. Down: Roe 2D

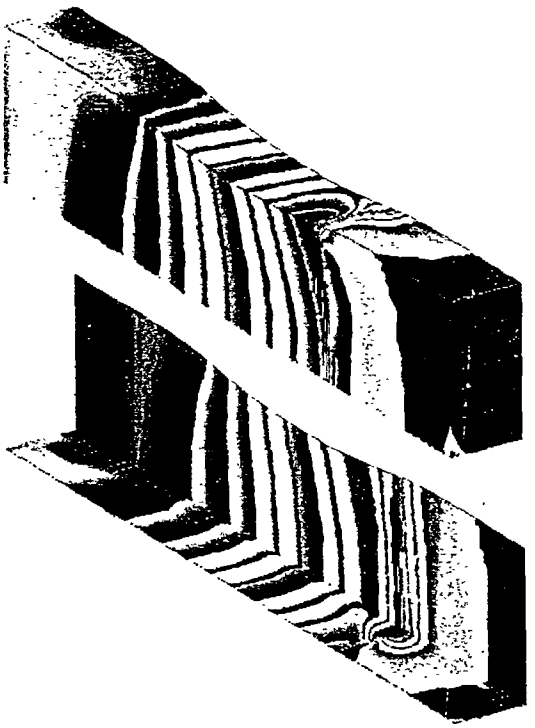

Figure 20 Turbulent three-dimensional iso-static pressure values

were used. This is an important result. Indeed, good agreement for inviscid computations is required, before considering the simulation of turbulent flows.

The next step was then a simulation of the two-dimensional interaction of the shock with the thin boundary layer developing on a bump. The core flows achieved were again similar, as well as the predicted boundary layer behaviour after the shock. Good agreement was obtained considering its rapid thickening and the downstream velocity recovery. However, slight discrepancies occurred in the main flow, near the outer edge of the boundary layer. These were strongly related to the way the turbulence model deals with the free stream turbulence.

The last step was to evaluate the behaviour of the unstructured method on the simulation of the whole three-dimensional nozzle. The results were close to the two-dimensional ones in the vertical plane of symmetry, and a large three-dimensional vortex was found in the upper right corner of the geometry, in the interaction zone of the shock with the two boundary layers. These numerical results must be confirmed by further comparisons between structured and unstructured methods. This is a work in progress.

ACKNOWLEDGEMENTS

The authors acknowledge support from CNRS, SNECMA and METRAFLU. Thanks are due to the C3NI team of CNUSC (Montpellier, France) where the structured computations† were done.

† The numerical results presented are freely available from the authors who invite further comparisons (E-Mail: aubert@mecaflu.ec-lyon.fr).

REFERENCES

1 Aubert, S., Hallo, L., Ferrand, P. and Buffat, M. Numerical behaviour of unsteady waves, *AIAA J.*, **33/5**, 888–893 (1995)
2 Adamson, T. C. and Liou, M. S. Unsteady motion of shock waves in two dimensional transonic channel flows, *Report No. UM-014534-F*, Department of Aerospace Eng., University of Michigan, Michigan, USA (June 1977)
3 Van Leer, B. Towards the ultimate conservative difference scheme V: a second-order sequel to Gudonov's method, *J. of Comput. Physics*, **32**, 101–136 (1979)
4 Parpia, I. H. Van Leer flux vector splitting in moving coordinates, *AIAA J.*, **26/2** (Jan. 1988)
5 Aubert, S. *Etude de schémas à haute précision pour la simulation d'écoulements transsoniques instationnaires ou visqueux. Application aux turbomachines*, PhD Thesis, Ecole Centrale de Lyon, France (1993)
6 Michel, R., Quemard, C. and Durant, R. *Application d'un schéma de longueur de mélange à l'etude des couches limites turbulentes d'équilibre*, ONERA, Note technique 154, Chatillon, France (1969)
7 Hirsch, C., *Numerical computation of internal and external flows Vol. 2*, John Wiley and Sons (1988)
8 Hallo, L., Brun, G., Souchet, M. and Aubert, S. Numerical simulation of viscous turbulent flow in transonic combustor, *Finite Elements in Fluids*, 498–507, Pineridge Press, Barcelona (1993)
9 Dervieux, A. Steady simulations using unstructured meshes, *VKI, Lecture series 1984-04* (1985)
10 Angrand, F. and Dervieux, A. Some explicit triangular finite element schemes for Euler equations, *Int. J. Num. Meth. in Fluids*, **4**, 749–764 (1984)
11 Launder, B. E. and Spalding, D. B. *Mathematical models of turbulence*, Academic Press, London (1972)
12 Le Ribault, C. *Simulation des écoulements turbulents compressibles par une méthode mixte éléments finis—volume finis*, PhD Thesis, Ecole Centrale de Lyon, France (1991)
13 Souffet, B. *Résolution numérique des équations d'Euler des fluides parfaits compressibles par des schémas implicites en éléments finis*, PhD Thesis, Université Paris VI, France (1984)
14 Hallo, L., Munier, J. L., Buffat, M. and Brun, G. Iterative methods for solving implicit non-structured finite volume discretization of Euler equations, submitted to publication to *Int. J. for Num. Meth. in Fluids* (1993)
15 Fezoui, F. and Stoufflet, B. *A class of implicit upwind schemes for Euler simulations with unstructured meshes*, Scientific report 517, INRIA (1986)
16 Bristeaux, M. O. and Periaux, F. Finite element methods for the calculation of compressible viscous flow using mesh refinement, *lecture notes in Comp. Fluid Dynamic, VKI* (1983)
17 Mulder, W. A. *Dynamics of gas in a rotating galaxy*, PhD Thesis, Roterdam (1985)
18 Cambier, L., Ghazzi, W., Veuillot, J. P. and Viviand, H. *Une approche par domaines pour le calcul d'écoulements compressibles*, ONERA, Note technique 143, Chatillon, France (1981)
19 Ott, P., Bölcs, A. and Fransson, T. H. Experimental and numerical study of the time-dependent pressure response of a shock wave oscillating in a nozzle, *ASME*, **93-GT-139** (1993)
20 Coquel, F. *Schéma de décomposition hybride, Cinquième séminaire sur les écoulements de fluides compressibles*, CEA, France (1993)
21 Van Leer, B. Flux vector splitting for the Euler equations, *Lecture Notes in Physics 170*, 501–512 (1982)
22 Thompson, K. W. Time dependent boundary conditions for hyperbolic systems, *J. of Comput. Physics*, **68**, 1–24 (1987)